Electrodeposited Cu_2O doped with Cl: Electrical and optical properties

S. Pelegrini, M. A. Tumelero, I. S. Brandt, R. D. Della Pace, R. Faccio, and A. A. Pasa

Citation: Journal of Applied Physics **123**, 161567 (2018); doi: 10.1063/1.5004782
View online: https://doi.org/10.1063/1.5004782
View Table of Contents: http://aip.scitation.org/toc/jap/123/16
Published by the American Institute of Physics

Electrodeposited Cu_2O doped with Cl: Electrical and optical properties

S. Pelegrini,[1,2] M. A. Tumelero,[2,3] I. S. Brandt,[1,2] R. D. Della Pace,[2] R. Faccio,[4] and A. A. Pasa[1,2,a)]

[1]*Programa de Pós-Graduação em Ciências e Engenharia de Materiais, UFSC, Florianópolis 88040-900, Brazil*
[2]*Laboratório de Filmes Finos e Superfícies, UFSC, Florianópolis 88040-900, Brazil*
[3]*Instituto de Física, UFRGS, C.P. 15051, 91501-970 Porto Alegre, RS, Brazil*
[4]*CentroNanoMat/CryssMat, DETEMA, Facultad de Química, UDELAR, Montevideo 11800, Uruguay*

(Received 15 September 2017; accepted 28 December 2017; published online 19 January 2018)

For understanding the electrical and optical properties of electrodeposited Cl-doped Cu_2O thin films, we have studied layers with increasing thickness and Cl concentrations of 0.8 and 1.2 at. %. The deposits were characterized by measuring the charge transport, the optical reflectance, and the photoluminescence. No significant decrease of electrical resistivity was observed in doped samples compared to undoped ones. A decrease of about five orders of magnitude was measured and ascribed to the presence of pinholes, as confirmed by scanning electron microscopy analyses. From optical measurements, we concluded that the Cl atoms are incorporated into substitutional sites of Cu_2O lattices in agreement with photoluminescence results showing a strong reduction in the peak intensity of V_O^{+2} defects in comparison to undoped layers. Computational calculation using density functional theory has pointed out high formation energy for single Cl related defects, but low formation energy for Cl-defect complexes, such as $Cl_O + V_{Cu}$, that strongly compensate the carriers generated by the Cl doping. *Published by AIP Publishing.*
https://doi.org/10.1063/1.5004782

I. INTRODUCTION

Cu_2O is a semiconductor that usually presents p-type conduction due to native point defects, mainly Cu vacancies.[1,2] The resistivity of this semiconductor, when prepared by electrodeposition, can vary in the range of 10^1 to 10^{11} Ω cm depending on the deposition parameters and incorporation of dopants.[3–8] Cu_2O is a relevant material for several applications such as photocatalysis[9] and solar cells (see Refs. 10 and 11, and therein), and it is very important to develop doping processes to reduce the resistivity and control the n and p character of the material. Considering the electrochemical doping, i.e., incorporation of dopants during growth of the layers, the doping of Cu_2O with Cl results in an oxide with n-type character and a very significant reduction of seven orders of magnitude in resistivity, as observed by Han *et al.*[4] The carrier inversion was also observed by other authors.[12,13] One hypothesis to explain the doping process is to assume that Cl promotes the formation of n-type layers by occupying an O site and introducing a donor level close to the bottom of the conduction band minimum (CBM). This assumption is in agreement with first-principles calculations done by Bai *et al.*[14] However, doping with Cl is a process that needs further investigation. In 2012, Lincot and co-workers[15] observed that Cl does not change the p-type character and the density of carriers when depositions occur at pH varying in the range of 9.0 to 12.5, at 60 °C and on F-doped SnO_2 substrates. A few years later, in 2015, Jayathilaka *et al.*[13] observed that the addition of Cl to the electrolyte resulted in Cu_2O deposits with n-type character and a monotonic decrease of 4 orders of magnitude in the resistivity as a function of $CuCl_2$ concentration at a pH of 9.3 and 60 °C on Ti substrates. In this case, the pH is much higher than the one used in Ref. 4 of 7.5, with the additional difference being that Jayathilaka *et al.*[13] used lower deposition potentials and lower Cl concentrations than in Ref. 15. Moreover, Biccari *et al.*[16] observed that in Cu_2O grown by thermal oxidation, Cl acts as a donor, substituting the oxygen, and as an acceptor when occupying interstitial positions. In a previous study, we have observed the influence of Cl on the structural and morphological properties of Cu_2O films for two Cl concentrations in the electrolyte.[17] In this work, chlorine doped Cu_2O samples were investigated looking for changes in the electrical resistivity (ρ), the refractive index (n) and the bandgap energy (E_g). The dependence of n and E_g on the thickness and amount of Cl is highlighted. Density functional theory (DFT) was used for understanding experimental data obtained from electrical, optical and photoluminescence (PL) measurements.

II. METHODS

Experimental: The electrodeposition of undoped and Cl-doped Cu_2O thin films was performed in a standard three-electrode electrochemical cell, with polycrystalline Au films as a working electrode, platinum foils as a counter electrode, and a saturated calomel electrode (SCE) as a reference electrode. The 50 nm thick Au working electrode was obtained by Au evaporation over a silicon (100) wafer. The Cu_2O films were produced by potentiostatic electrodeposition with three distinct electrolytes with 0.4 M copper sulfate, 3.0 M lactic acid and copper chloride (none, 0.01 and 0.1 M for

a)andre.pasa@ufsc.br

each electrolyte). The pH of 7.5 was controlled by adding sodium hydroxide to the electrolyte. During Cu_2O deposition, the temperature was 60 °C, and the applied potential was maintained at −0.2 V. The presence of Cl in amounts of 0.6 and 1.2 at. % for low (0.01 M) and high (0.1 M) concentrated solutions, respectively, was observed in the Cu_2O layers close to the interface of Cu_2O/Au. The Cl concentration decreases slowly along the deposited layer reaching lower values at the surface, as observed in our previous work.[17] The usual two probe method was used to measure the resistivity of the samples. The measurements were done as a function of temperature through the thickness of the layers using the gold substrate as one contact and silver paste on top as other one, both forming ohmic contacts to Cu_2O. The morphology was investigated by Scanning Electron Microscopy (SEM) with a Helios 450S (FEI). The photoluminescence (PL) experiments were done in a homemade setup using a 266 nm laser with an intensity of 5 mW. The optical properties were determined from the optical reflectance spectra (R) over the wavelength range λ of 250 to 2500 nm, recorded using a Perkin-Elmer Lambda 750 spectrometer with an integration sphere of 60 mm. The bandgap was obtained by using the Tauc method.

Computation: The DFT based calculation was performed in the VASP package[19] using a plane wave basis and a PAW method.[20] The structural optimization of the cells was done with the GGA + U method using the PBE functional,[19] while the electronic and energy calculations were done with a hybrid method using the HSE functional;[21] in all cases, the tolerance in forces was selected as 0.01 eV/Å and 1 kbar in the stress tensor components. An additional U_{eff}=U-J onset energy of 5.2 eV was applied to the Cu-d orbital on the basis of Dudarev approach,[22] even for HSE calculations, as previously proposed.[23] The GGA + U method corrects the valence band shift due to localization effects,[24] while the hybrid functional corrects the conduction band shift and consequently the bandgap value. The HSE functional leads to a bandgap of 1.9 eV,[14] slightly underestimated in comparison to experimental 2.1–2.2 eV values. Scanlon and Watson[25] have corrected this problem by increasing the exact Hartree exchange fraction in the HSE06 functional to 27.5% (instead of 25%, as proposed originally in Ref. 21). Here, the utilization of HSE with the GGA + U xc-functional instead of GGA leads to an exact 2.17 eV bandgap without changing the 25% of the exact exchange part. The energy cutoff for the plane wave expansion was 400 eV for all atoms, and a k-mesh of 4 × 4 × 4 was used for the electronic and energy calculations. The formation energies were calculated as described elsewhere.[8] Equilibrium conditions were based on the pH of an aqueous environment, as previously reported[8] and similar to Ref. 26.

III. RESULTS AND DISCUSSION

A. Electrical measurements

In Fig. 1 is presented the procedure for electrical measurements. We have used electrical contacts with large (3 mm^2) and small (0.5 mm^2) areas, as shown in Figs. 1(a) and 1(b), respectively. The idea is to check for the presence of defects that could short-circuit the Cu_2O layers such as pinholes, large defects and cracks. As described above, resistivity is measured with 2 contacts, one on the bottom and the other one on the top, as illustrated.

Figure 2 shows the resistivity as a function of the temperature for the sample with higher content of Cl (1.2 at. %) for the small and large area electric contacts. As can be seen, the large area contacts present resistivity in the range of 10^3 Ω cm with increasing values when raising the temperature, a typical behavior of metals. This behavior is certainly due to the formation of short circuits between top and bottom contacts due to filling of pinholes and extended defects with silver paste from the top contact. By reducing the size of the top contact, it was possible to find regions free of defects where the resistivity showed much higher values of ca. 10^7 Ω cm at room temperature, and temperature dependence typical for semiconductors, as shown in the figure.

Since for large area contacts we have observed the behavior that is related to the presence of metallic short circuits, we have used scanning electron microscopy (SEM) to find the presence of large defects and pinholes. Figure 3 shows a high-magnification image revealing the presence of pinholes with diameters of less than 50 nm. Figure 3(a) shows a region with many pinholes and Fig. 3(b) shows the enlargement of the area defined in Fig. 3(a) by the square with just one pinhole inside. In our case, the reduction of 5 orders of magnitude in the resistivity shown in Fig. 2 could be explained by the presence of these pinholes.

From contacts with small size on regions free of defects, i.e., areas with very high resistivity, we have obtained the resistivity as a function of temperature in the range of 200 to

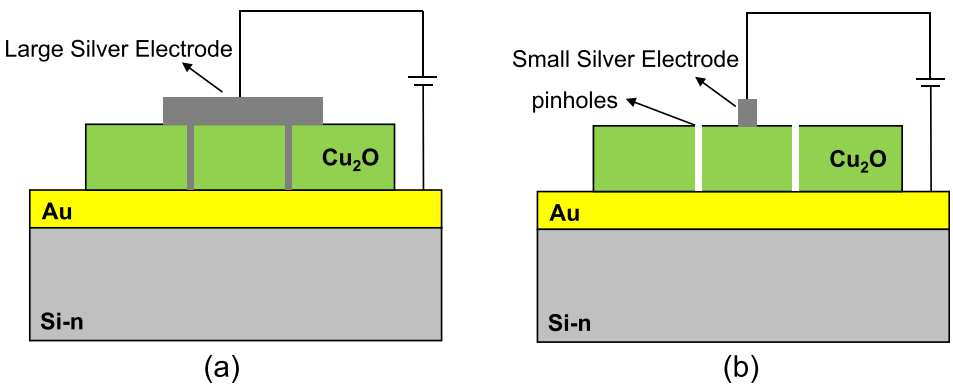

FIG. 1. (a) Large (3 mm^2) and (b) small (0.5 mm^2) area contacts for measuring the electrical resistivity of the Cu_2O layers.

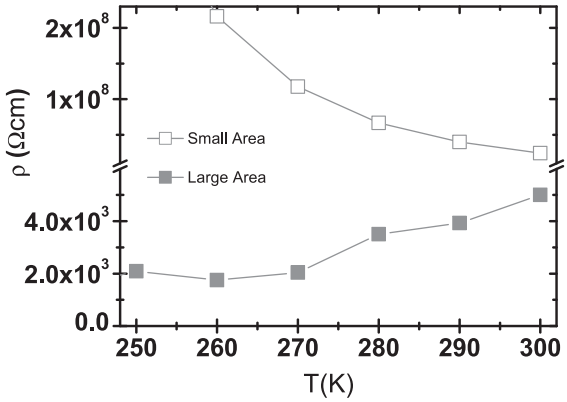

FIG. 2. Resistivity *vs*. temperature for two different contact areas for a Cu_2O sample with 0.1 M $CuCl_2$ and 600 nm thickness.

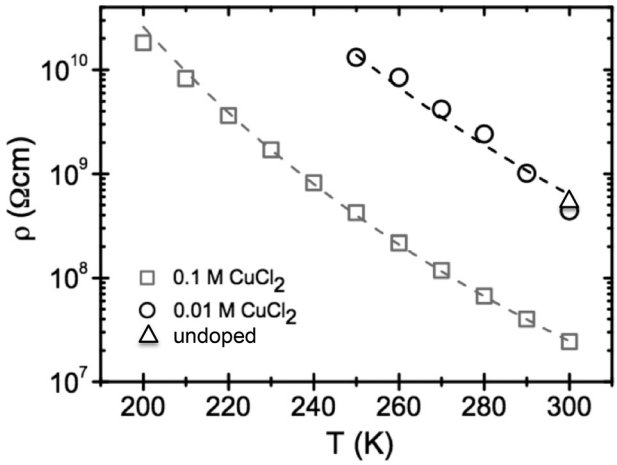

FIG. 4. Resistivity of Cu_2O layers as a function of temperature for 0.6 and 1.2 at. % of Cl and for the undoped sample at room temperature.

300 K for samples with low (0.6 at. %) and high (1.2 at. %) content of Cl, as can be seen in Fig. 4. The thickness of the samples is 600 nm. The sample with 0.6 at. % showed the same resistivity value as undoped ones at room temperature. The increase in Cl concentration reduced the resistivity by more than one order of magnitude. The activation energies were obtained by fitting exponentially the data using an Arrhenius-like expression, shown by the dashed lines in Fig. 4. Both samples show almost same thermally activated behavior, typical for deep electronic doping levels and with activation energies of about 0.40 and 0.36 eV for lower and higher concentrations of Cl, respectively, which are presumably donor levels since it is an n-type material. These values of activation energy are deeper in band gap than the theoretical values found in Ref. 14 for donor levels induced by chlorine in substitutional oxygen sites; moreover, the bandgap obtained in this reference is smaller than the experimental one. The most important point in these electrical transport experiments is the high values of resistivity found, that are in disagreement with existing data in the literature.[4,12,13] The use of a small area contact was an important step to obtain reproducible data with semiconducting behavior.

B. Optical properties

The reflectance of the samples was measured in the wavelength (λ) range of 250 to 2500 nm, and the n was calculated from the observed oscillations.[27] Figures 5(a) and 5(b) show n versus λ for films with different thicknesses for both concentrations of Cl, that is, 0.6 and 1.2 at. %, respectively. The rapid decrease of n close to $\lambda \sim 500$ nm is a signature of the Cu_2O band gap. In the transparent region, for λ higher than ~1000 nm, n becomes constant. In Fig. 5(c) are plotted the n values extracted at $\lambda = 1500$ nm versus the film thickness for undoped and doped samples. The n values are higher for the sample with a higher amount of Cl, and decreases with thickness, varying from 2.4 to 1.8. A similar behavior has been observed for p-type Cu_2O thin films.[18] For the undoped sample, n reaches a constant value with the thickness. It is important to make clear that the behavior of n as a function of Cl doping and film thickness is not related to porosity created by pinholes. From cross-section and plane view SEM images (not shown), it was observed that pinholes represent a very small portion of the Cu_2O film and there is no appreciable density variation of pinholes while comparing undoped and doped films of different thicknesses. The short circuit in the electrical measurements is observed when the electrical contacts are on top of regions with pinholes, and for contacts with 0.5 mm^2 it is possible to find regions free of pinholes, as inferred from the results in Fig. 2.

A better understanding regarding the behavior of n as a function of doping level and thickness can be achieved using the Wemple and DiDomenico (WD) model.[28] This model considers a single effective oscillator with energy E_m that describes the interband transition (also known as the Sellmeier gap) and a parameter E_d, called dispersion energy,

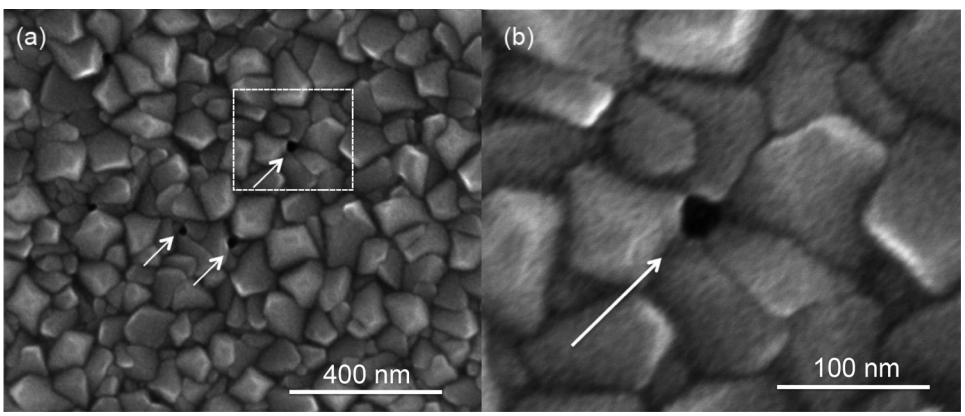

FIG. 3. (a) SEM top-view image of a film with pinholes. (b) Magnification of the area delimitated by the dashed square in (a) showing a pinhole with a diameter of ~40 nm.

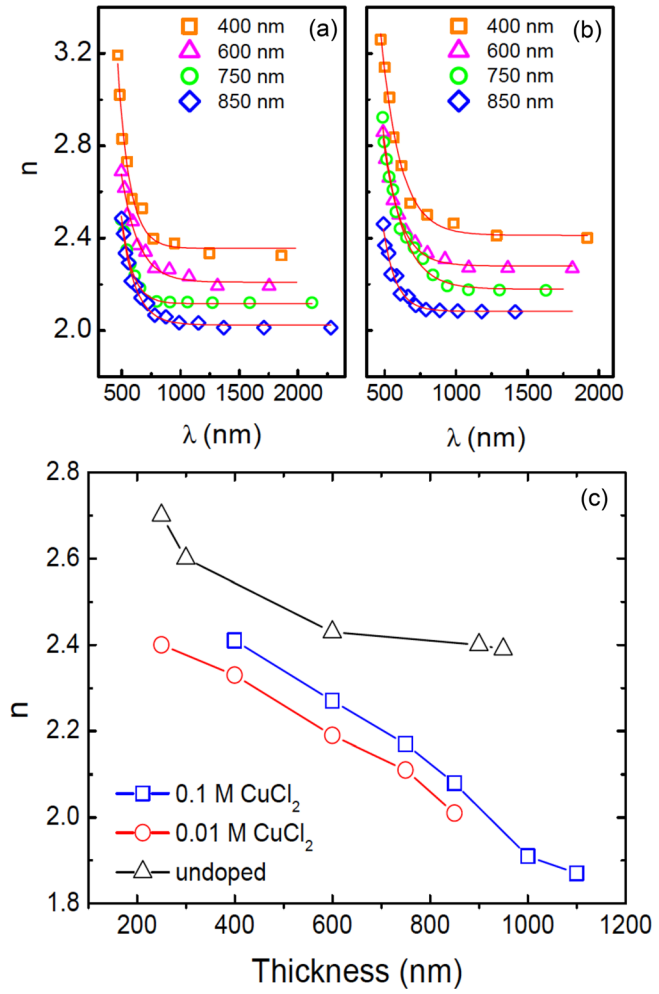

FIG. 5. Refractive index vs. wavelength for Cu_2O films with different thicknesses deposited with (a) 0.01 and (b) 0.1 M $CuCl_2$. (c) Refraction index at $\lambda = 1500$ nm vs. thickness of Cu_2O doped and undoped films.

that measures the average strength of the interband optical transition.[28,29] E_d depends on the effective mass of the electronic cloud surrounding each atom and the electrical charge of that cloud. Since these quantities are affected by crystalline distortions/imperfections, as point defects, E_d can give a picture of the density of defects in the material.[18,30] The procedure to calculate E_m and E_d is described in Refs. 18 and 28.

In Figs. 6(a) and 6(b) are plotted E_m and E_d against the thickness of the layers for undoped and doped films. The oscillator energy E_m is independent of the thickness, and an average value of 3.6 eV is observed. Based on the WD model, the E_m value allows calculating a band gap energy of about 2.2 eV that is very close to the value of Cu_2O. The E_d values are lower for Cl doped than for undoped films. Moreover, for doped films, E_d decreases significantly with thickness reaching values close to 8.3 eV, which is the expected value for stoichiometric Cu_2O crystals using the WD model.

The strong dependency of E_d on the thickness suggests that the electronic structure of Cu_2O changes as it grows, probably due to a reduction in the defect concentration, which is in agreement with the amount of incorporated Cl that decreases from the interface to the surface of the layers, as observed previously.[17] The Cl ions occupying the existing O vacancies could reduce electronic disorder. This hypothesis is supported by data for undoped layers in Fig. 6(b), where the initial and final E_d values are much higher than for the doped ones.

The dependence of n and E_d on the doping level is not equally observed in the electrical resistivity results (Fig. 4). It is an indication that Cl doping modifies the electronic structure of Cu_2O, but the related defect states are not electrically active as will be further discussed in this manuscript.

From reflectance data, we have also obtained the absorption coefficient and calculated the Tauc direct energy gap of doped and undoped layers, as shown in Fig. 6(c). It is noted that E_g does not depend on film thickness and Cl doping, the same happening to E_m as expected since E_m can also be calculated directly from E_g in the WD model.

C. Photoluminescence

Figure 7(a) presents the photoluminescence (PL) spectra of 600 nm thick Cu_2O thin films with different chlorine

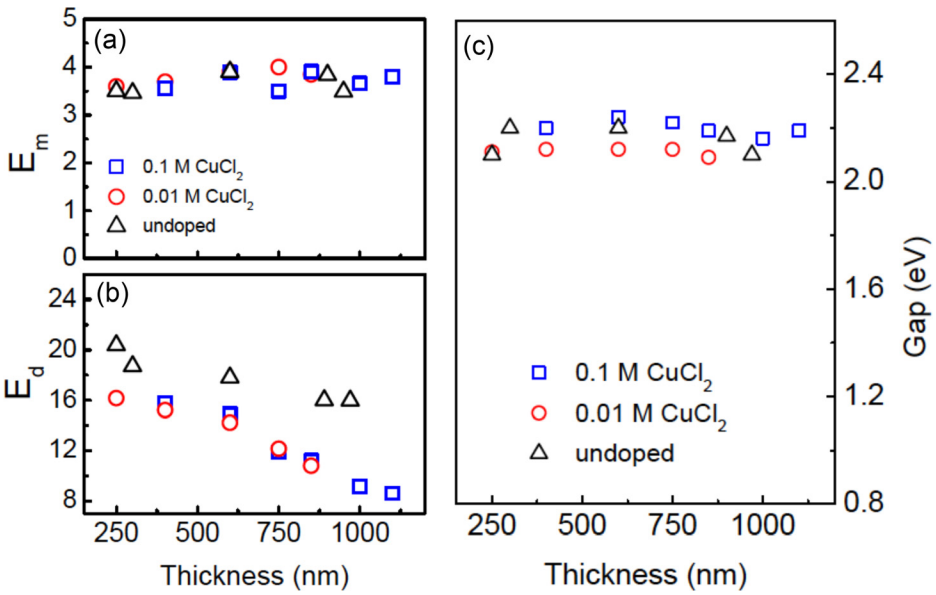

FIG. 6. (a) E_m, (b) E_d and (c) E_g as a function of Cu_2O film thickness for doped and undoped samples.

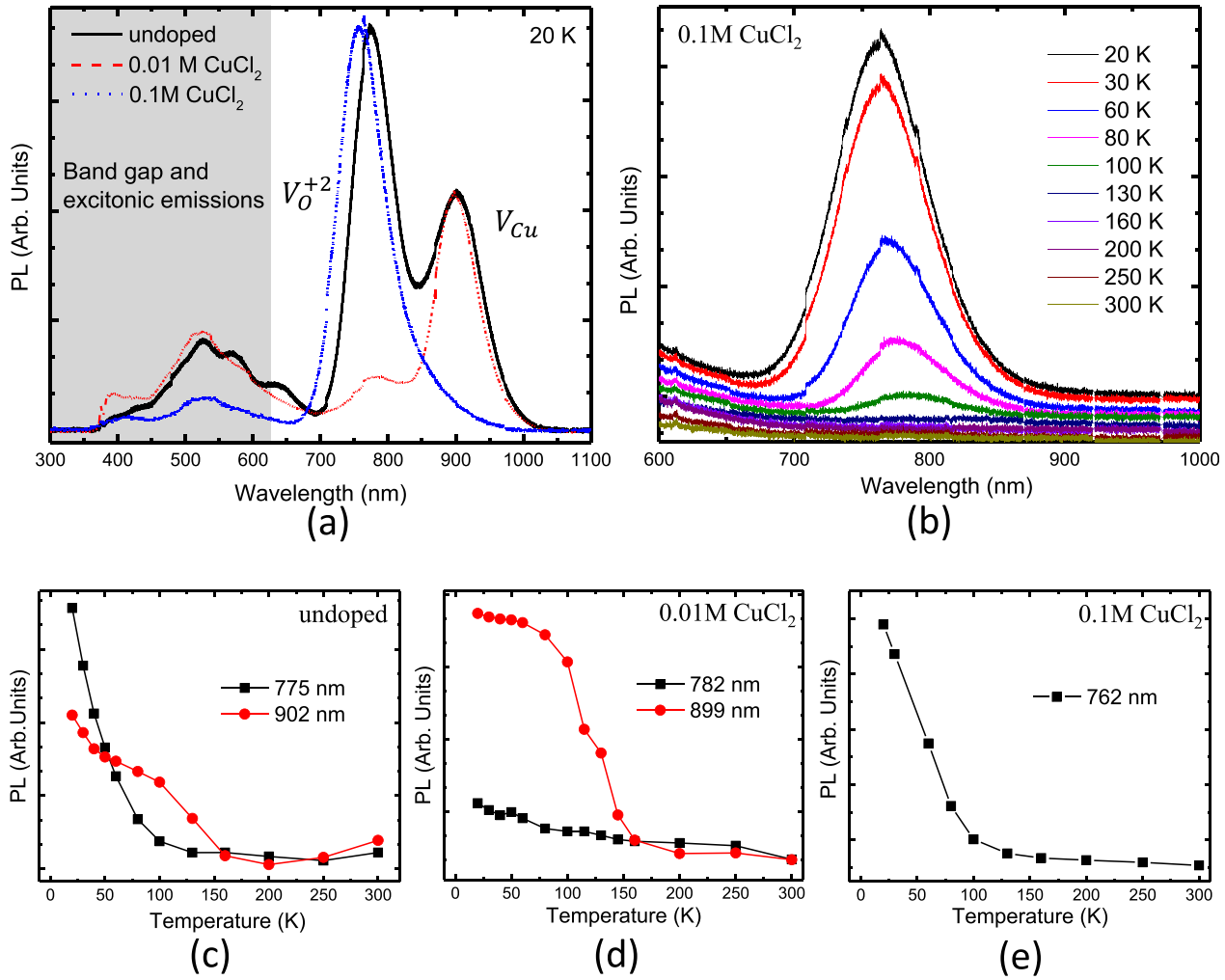

FIG. 7. Photoluminescence spectra of Cu_2O thin films: (a) undoped, and with 0.01 M and 0.1 M $CuCl_2$ in the solution. (b) Photoluminescence spectra of Cu_2O thin films with 0.1 M $CuCl_2$ in the solution as a function of temperature. The temperature profiles of peak intensities of samples: (c) undoped, and with (d) 0.01 M and (e) 0.1 M $CuCl_2$ in the solution.

concentrations, measured at 20 K. It has been determined previously that apart from the excitonic emissions with energy near the bandgap,[31] three other emissions can be found with energies lying deep in the band gap and due to radioactive processes related to point defects induced electronic levels.[32] One of these levels is attributed to copper vacancies, V_{Cu}, emitting light with an energy of about 1.36 eV ($\lambda = 910$ nm),[32,33] while the other two are attributed to oxygen vacancies, V_O, occurring at 720 nm and 820 nm, the former due to doubly ionized vacancy and the later due to single ionized defects.[32] The relative intensity of such emissions depends on the synthesis methodology.[33] For the undoped samples in Fig. 7(a), two PL peaks can be seen at about 775 and 902 nm due to electronic levels V_O^{+2} and V_{Cu}. Since the deposition pH is low (7.5), a predominance of V_O defects is expected due to its lower formation energy in pure Cu_2O, as will be discussed below, and also from the previous calculation.[14] For doped samples with 0.6 at. % Cl, the PL spectrum still presents the two vacant emissions, but the peak intensity of V_O^{+2} is strongly reduced in comparison to undoped samples, indicating that the density of V_O has decreased by doping. Such a result is consistent with the Cl occupation of oxygen vacant sites, as discussed above. Similar results were found in N doped Cu_2O.[34] For the samples with 1.2 at. %, the V_{Cu} peak vanishes and the peak V_O appears with high intensity shifted to lower wavelengths (~762 nm), as seen in Fig. 7(a). The shift and intensity increase of V_O in the highly-doped samples can be discussed in terms of two hypotheses; first, the possibility of Cl forming defect complexes with copper vacancies,[35,36] which will be discussed further in this text, and second, the fact that the growth dynamics is affected by the addition of $CuCl_2$ in the electrolyte,[17] making the deposition faster and thereby propitiating the formation V_O. The first hypothesis seems to be more promising since the disappearance of the V_{Cu} peak could be explained by the formation of a defect complex with Cl, that is more concentrated in the deposit.

In Fig. 7(b) is displayed the PL spectra for 1.2 at. % Cl, measured at different temperatures. By increasing the temperature, the peak amplitude rapidly decreases, up to 100 K, vanishing beyond that. In all temperatures, just a single peak is observed. The temperature profiles of peak intensity are presented in Figs. 7(c), 7(d), and 7(e), for undoped, 0.6 and 1.2 at. % Cl, respectively. For the undoped sample, Fig. 7(c), and a less Cl concentrated sample, Fig. 7(d), the two observed peaks are thermally activated with different

temperature behaviors. The peak at about 780 nm, indexed to V_O^{+2}, falls quickly when the temperature is raised, while the peak at about 900 nm, due to V_{Cu}, starts to decrease above 100 K and disappears at about 200 K resembling a freeze-out behavior. The freeze-out behavior of the V_{Cu} peak may be related to the existence of bound excitons with a binding energy of about 60 meV (activation energy obtained from the Arrhenius plot). In Fig. 7(e), there are two main differences in comparison to 7(c) and 7(d); the peak at about 900 nm does not appear and the peak for Vo presents a slight blue shift to 762 nm.

D. DFT calculations

Figure 8(a) shows the formation energy of different neutral defects and dopant conformations, as a function of the pH of the growing environment, calculated using DFT methodology described in Sec. II. Naturally, at low pH, the defects ruling the system (with smaller formation energy) are the ones that are oxygen-deficient, such as oxygen vacancies (V_O) and copper interstitials (Cu_{int}^{tet} and Cu_{int}^{oct}, Cu interstitials in tetrahedral and octahedral sites, respectively), while at basic pH, oxygen-excess defects occur at higher concentrations, such as Cu vacancies (V_{Cu}). The antisite defect Cu_o, Cu occupying an O site, presents high formation energy and should occur in low concentrations in either pH situations. This diagram shows that in the absence of chlorine dopants, the most relevant defects are vacancies. Here, the calculated formation energy for Cl_O (Cl occupying an O site) reveals itself being expensive, ranging between 3 and 5 eV, much higher than V_O, for instance. At basic pH, Cl atoms occupying interstitial sites (Cl_{int}^{tet} and Cl_{int}^{oct}, Cl interstitial in tetrahedral and octahedral sites, respectively) present smaller formation energies than the substitutional ones (Cl_O), pinning the Fermi level at the middle of the bandgap, since such interstitial dopants introduce deep donor levels [see Fig. 8(b)].

When calculating the formation energy of Cl dopants, the choice of the host is important; here, we choose a perfect Cu_2O cell. When pH is raised, the Cl_O formation energy increases due to the high energy cost to remove an oxygen from the cell. A significant reduction of the formation energy of Cl_O occurs when a Cu vacancy (V_{Cu}) is added to the vicinity of the dopant (i.e., a copper neighbor is removed), as can be seen by the line for Cl_O* ($Cl_o + V_o$ complex) in Fig. 8(a), which is almost independent of the pH. It occurs because the removal of an extra atom allows better relaxation of the surrounding ions and compensates the pending bond of Cl. This indicates that Cl doping (at high concentration, ~2% used in the calculations) should increase the concentration of defects such as V_{Cu}. Calculation using a more diluted supercell was not done due to computational limitations.

In Fig. 8(b), each line corresponds to one type of defect, the change in the inclination stands for a transition level in which the charge state of the defect is modified. First, one can see that no transition level is found for V_O as expected,[2,21] implying that V_O should not donate electrons to the conduction band nor contribute to n-type behavior of undoped Cu_2O. The methodology used here led to shallower levels than the ones obtained in Ref. 21. Here, an acceptor transition level at about 0.15 eV above the valence band maximum (VBM) was found for V_{Cu}, while copper interstitials induce shallow delocalized host donor levels resonant in the conduction band. These copper interstitial levels can explain the natural n-type conduction of Cu_2O found experimentally for depositions at low pH.[25] The copper antisites, otherwise, present very high formation energies and could be discarded as a source of carriers. Substitutional doping with Cl atoms (Cl_O) also introduces shallow donor levels near the conduction band, seen by the positively charged state over the entire bandgap in Fig. 8(b). The Cl in interstitial sites (Cl_{int}^{tet} and Cl_{int}^{oct}) introduces deep acceptor levels in the bandgap at about 0.6 and 1.1 eV, respectively, compensating and scattering the charge carriers. Considering Cl_O^* ($Cl_O + V_{Cu}$ complex), a very deep transition level is found at about 0.22 eV above the VBM; the presence of the vacancy completely compensates the shallow donor of Cl_O, as will be discussed below.

Figure 9 presents the density of states (DOS) for different defects and dopant configurations. In the shaded gray area is displayed the DOS for the pure host. In Fig. 9(a), the DOS for the V_{Cu} defect shows a peak at about 0.18 eV above the VBM (indicated by the arrow), close to the energy found for the V_{Cu} transition level in Fig. 8(b). The DOS indicates that this state is mostly formed by Cu orbitals rather than oxygen. In Fig. 9(b), the DOS for the V_O defect shows an empty band gap. In Fig. 9(c), the DOS of a chlorine doped cell (Cl_O) is presented, showing a few states near the CBM (indicated by the arrow), as expected due to shallow donors. Notwithstanding, these shallow donors are not formed by Cl

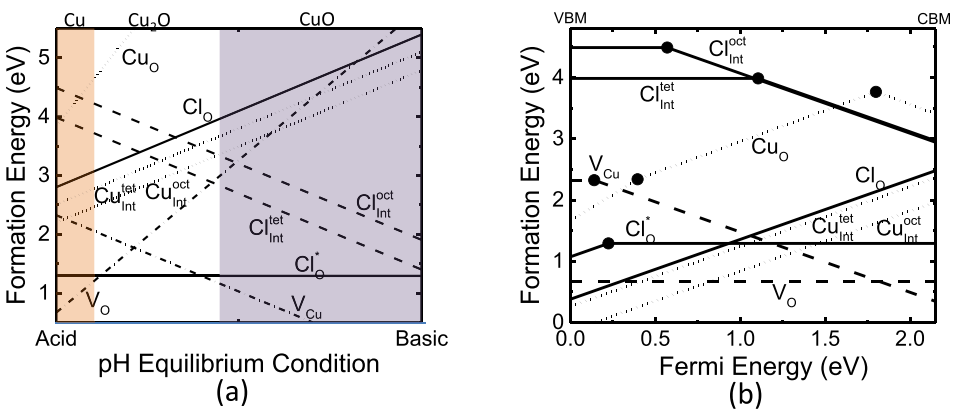

FIG. 8. (a) Diagram of formation energy vs. pH, each line represents one type of defect/dopant. (b) Graph of the formation energy vs. Fermi energy for the calculated defects/dopants, the dots stand for the transition levels inside of the bandgap.

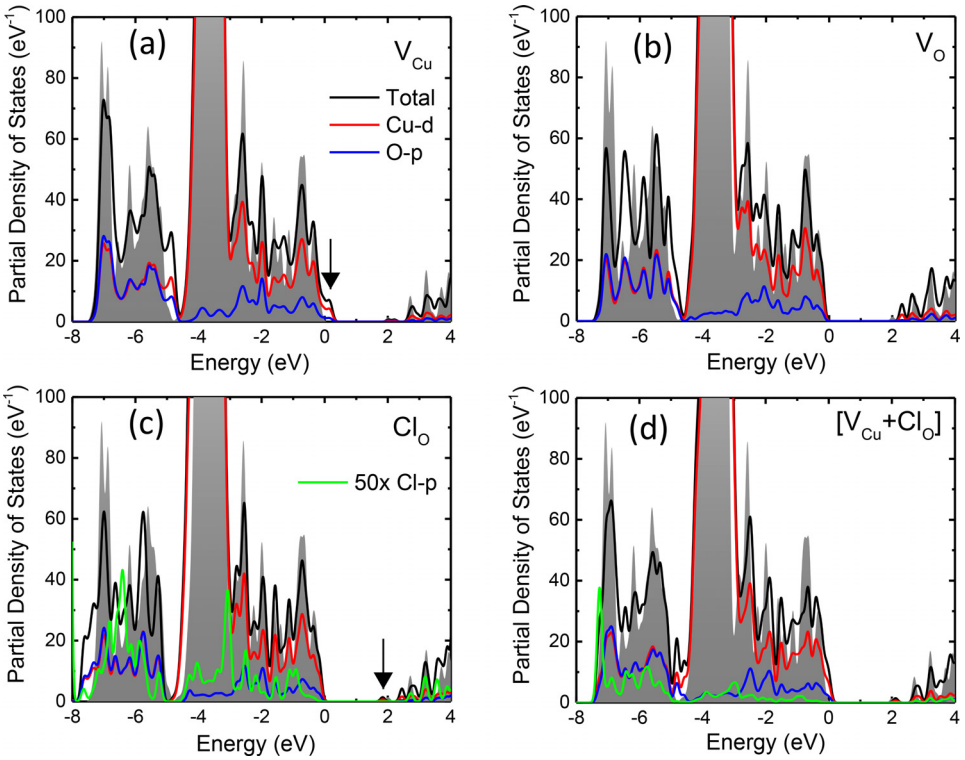

FIG. 9. Partial and total densities of states calculated for different defect/dopant conformations: (a) for a copper vacancy, (b) for an oxygen vacancy, (c) for a chlorine in an oxygen site and (d) for a coupled Cu vacancy and a chlorine substituting an oxygen.

orbitals, that appear just at high energies, suggesting that such levels are typical host delocalized levels. Additionally, one can see that the p-orbitals of Cl are overlapped by the d-orbital of Cu, denoting a strong coupling between these atoms. Finally, Fig. 9(d) displays the DOS for the $Cl_O + V_{Cu}$ complex, showing reduced hybridization between Cu and Cl orbitals.

E. Discussion of electrical and optical experiments versus theory

Since experimental reports have shown that n-type Cu_2O can be obtained by either electrodeposition in acid (low pH) or by extrinsic doping with chlorine, the overall debate is about the origin of the carriers in n-type Cu_2O. It has been agreed that V_O cannot generate such electron carriers, since it stays neutral inside the bandgap, see Fig. 8(b) and Ref. 25. Nevertheless, based on the methodology applied in this work, the Cu atoms in interstitial sites seem to generate shallow donors, but would exist in small concentrations due to the high formation energy, so it is reasonable to assume that only under very low pH conditions they could contribute to the conduction, which corroborates with the experimental data discussed above, where intrinsic n-type conduction has been found only at acid/neutral pHs.[10,25] Regarding Cl doping, the experimental result presented here shows that no relevant reduction in the resistivity is achieved. Looking at DFT data, Cl_O shall introduce shallow donor levels in Cu_2O, but if Cl stays in an interstitial site (Cl_{int}^{tet} and Cl_{int}^{oct}) it just compensates carriers due to deep acceptor levels. Both substitutional and interstitial doping sites present similar formation energies and defect concentrations that imply carrier compensation. In addition, the existence of defect-dopant complexes cannot be neglected, in which the carriers are fully compensated, reducing the conductivity. The presence of dopant-defect complexes in Cu_2O has been previously reported.[8,35,36] Nonetheless, the origin of the carriers remains unclear; once, no transition levels were found with first principles calculation that fits the activation energy obtained with electrical experiments from Sec. III A of 0.36 and 0.40 eV. However, we speculate from the close values of electrical resistivity of low Cl-doped and undoped samples at room temperature that the n-type found experimentally could be related to Cu interstitial defects rather than chlorine dopants. The reduction in the Cu_2O resistivity with Cl doping, shown in Fig. 4, can be attributed to the presence of uncompensated Cl dopants in the Cu_2O lattice or changes in morphology caused by the higher $CuCl_2$ concentration in the electrolyte that reduced the grain size of the deposits, as observed in our previous work.[17]

The refractive index and photoluminescence measurements lead to the same conclusion that under low Cl doping a reduction in the defective sites occurs, which can be seen as an overall reduction of the electronic disorder. By further doping, as in the case of 1.2 at. %, the number of defects increases slightly in comparison to that of 0.6 at. %. The PL characterization points to a large decrease of oxygen vacancies from being undoped to 0.6 at. % doped samples, which are non-electrical active defects (DFT analysis), in agreement with transport results, where no changes in electrical resistivity are observed. At high doping concentrations, the strong peak found at about 760 nm in the PL spectrum can be discussed in two terms; an enhancement in oxygen vacancy concentration which is not related to Cl doping, but due to changes in growth dynamics. The second possibility, which seems to be more consistent with computational results, is the rise of defect complex amount due to the high concentration of Cl. The DFT results of the $Cl_O + V_{Cu}$

complex in the Cu_2O cell support the existence of a deep level at about 0.22 eV; such level can host an electron transition from a conduction band (or from an excitonic level) emitting light with wavelengths at about 760 nm. The presence of high concentration of such defect complexes, which shall occur in highly chlorine doped samples, could increase the electronic disorder as well, raising the refractive index, in agreement with what was found experimentally for 1.2 at. % Cl. Therefore, optical characterization shows that Cl doping induces changes in the Cu_2O defect related electronic structure; however, such defect states are not electrically active.

IV. CONCLUSIONS

In summary, the refractive index suffered a sharp decline, reaching 1.8 for films with a thickness of 1100 nm; this is the smaller n found in the literature for Cu_2O thin films. On the other hand, the Cu_2O band gap suffered a weak variation with Cl concentration in the solution and no variation with film thickness. By using Wemple-Didomenico analysis, it was possible to observe that as thickness increases, the defect density decreases. Although E_d values are very high in thinner films, for thicker films, these values decrease almost linearly, reaching the expected value for bulk Cu_2O. We also showed that Cu_2O-Cl electrical resistivity does not decrease significantly in comparison to undoped samples, being the slight observed reduction associated with a few uncompensated Cl dopants or changes in the Cu_2O film structure. A decrease by about five orders of magnitude may come from the presence of pinholes in the films, as concluded from electrical measurements with 2 different contact areas. The occupation of non-electrical active oxygen vacancies by Cl atoms was observed by photoluminescence analysis. Computational calculation using DFT approach has pointed out high formation energy for Cl related doping, but low formation energy for Cl-defect complexes, such as Cl_O+V_{Cu}, that strongly compensates the carriers generated by the Cl doping. Therefore, electrical measurements and DFT calculations corroborate that Cl doping is not able to induce a reduction in the Cu_2O resistivity of several orders of magnitude.

ACKNOWLEDGMENTS

We offer our thanks to the Brazilian agencies CNPQ, CAPES, FAPESC, and FINEP for providing additional support to this work. The authors also thank Professor A. N. Klein for using the Raman facilities in the LABMAT/UFSC. The SEM images with the Helios 450S (FEI) microscope were obtained at the INL (Braga, Portugal) facilities. R.F. acknowledges CSIC, PEDECIBA, and ANII for financial support. All the computational calculations were done in the CENAPAD-SP cluster at Campinas/SP.

[1]A. N. Banerjee and K. K. Chattopadhyay, Prog. Cryst. Growth Charact. Mater. **50**, 52 (2005).
[2]H. Raebiger, S. Lany, and A. Zunger, Phys. Rev. B **76**, 45209 (2007).
[3]N. G. Elfadill, M. R. Hashim, K. M. Chahrour, and S. A. Mohammed, Semicond. Sci. Technol. **31**, 065001 (2016).
[4]X. Han, K. Han, and M. Tao, Electrochem. Solid-State Lett. **12**, H89 (2009).
[5]K. Mizuno, M. Izaki, K. Murase, T. Shinagawa, M. Chigane, A. Tasaka, and Y. Awakura, J. Electrochem. Soc. **152**, C179 (2005).
[6]T. Mahalingam, J. S. Chitra, S. Rajendran, M. Jayachandran, and M. J. Chockalingam, J. Cryst. Growth **216**, 304 (2000).
[7]A. E. Rakhshani, J. Appl. Phys. **69**, 2365 (1991).
[8]I. S. Brandt, M. A. Tumelero, E. Lima, L. Douglas, R. D. Zysler, R. Faccio, and A. A. Pasa, J. Magn. Magn. Mater. **441**, 374 (2017).
[9]A. Paracchino, V. Laporte, K. Sivula, M. Grätzel, and E. Thimsen, Nat. Mater. **10**, 456 (2011).
[10]I. S. Brandt, M. A. Tumelero, S. Pelegrini, G. Zangari, and A. A. Pasa, J Solid State Electrochem. **21**, 1999 (2017).
[11]R. Wick and S. D. Tilley, J. Phys. Chem. C **119**, 26243 (2015).
[12]S. Pelegrini, C. I. L. de Araujo, R. C. da Silva, A. D. C. Viegas, and A. A. Pasa, ECS Trans. **31**, 143 (2010).
[13]K. M. D. C. Jayathilaka, A. M. R. Jayasinghe, G. U. Sumanasekara, V. Kapaklis, W. Siripala, and J. K. D. S. Jayanetti, Phys. Status Solidi Basic Res. **252**, 1300 (2015).
[14]Q. Bai, W. Wang, Q. Zhang, and M. Tao, J. Appl. Phys. **111**, 23709 (2012).
[15]S. Haller, J. Jung, J. Rousset, and D. Lincot, Electrochim. Acta **82**, 402 (2012).
[16]F. Biccari, C. Malerba, and A. Mittiga, Sol. Energy Mater. Sol. Cells **94**, 1947 (2010).
[17]S. Pelegrini, I. S. Brandt, C. C. P. Cid, E. A. Isoppo, A. D. C. Viegas, and A. A. Pasa, ECS J. Solid State Sci. Technol. **4**, P181 (2015).
[18]I. S. Brandt, C. A. Martins, V. C. Zoldan, A. D. C. Viegas, J. H. Dias Da Silva, and A. A. Pasa, Thin Solid Films **562**, 144 (2014).
[19]J. P. Perdew, K. Burke, and M. Ernzerhof, Phys. Rev. Lett. **77**, 3865 (1996).
[20]P. E. Blochl, Phys. Rev. B **50**, 17953 (1994).
[21]J. Heyd, G. E. Scuseria, and M. Ernzerhof, J. Chem. Phys. **118**, 8207 (2003).
[22]S. L. Dudarev, G. A. Botton, S. Y. Savrasov, C. J. Humphreys, and A. P. Sutton, Phys. Rev. B **57**, 1505 (1998).
[23]M. Aras and C. Kılıç, J. Chem. Phys. **141**, 44106 (2014).
[24]D. Scanlon, B. Morgan, G. Watson, and A. Walsh, Phys. Rev. Lett. **103**, 96405 (2009).
[25]D. O. Scanlon and G. W. Watson, J. Phys. Chem. Lett. **1**, 2582 (2010).
[26]W. Wang, D. Wu, Q. Zhang, L. Wang, and M. Tao, J. Appl. Phys. **107**, 123717 (2010).
[27]J. Torres, J. I. Cisneros, G. Gordillo, and F. Alvarez, Thin Solid Films **289**, 238 (1996).
[28]S. H. Wemple and M. DiDomenico, Phys. Rev. B **3**, 1338 (1971).
[29]R. D. Shannon, R. C. Shannon, O. Medenbach, and R. X. Fischer, J. Phys. Chem. Ref. Data **31**, 931 (2002).
[30]A. L. J. Pereira and J. H. D. da Silva, J. Non. Cryst. Solids **354**, 5372 (2008).
[31]J. I. Jang, Y. Sun, B. Watkins, and J. B. Ketterson, Phys. Rev. B **74**, 235204 (2006).
[32]T. Ito and T. Masumi, J. Phys. Soc. Jpn. **66**, 2185 (1997).
[33]J. Bloem, A. J. Van der Houven van Oordt, and F. A. Kroger, Physica **22**, 1254 (1956).
[34]J. Li, Z. Mei, L. Liu, H. Liang, A. Azarov, A. Kuznetsov, Y. Liu, A. Ji, Q. Meng, and X. Du, Sci. Rep. **4**, 7240 (2014).
[35]M. Nolan and S. D. Elliott, Chem. Mater. **20**, 5522 (2008).
[36]L. Y. Isseroff and E. A. Carter, Chem. Mater. **25**, 253 (2013).